

## Supporting Information

### **Reconfigurable Double-Sided Smart Textile Circuit with Liquid Metal**

Chanho Jeong,<sup>a,b</sup> Ki Yoon Kwon,<sup>b</sup> Di Wu,<sup>c</sup> Yibo Fu,<sup>c</sup> Yeong-sinn Ye,<sup>b</sup> Sang Gil Lee,<sup>d</sup> Beomchan Kang,<sup>a</sup> Lining Yao,<sup>e</sup> Tae-il Kim\*<sup>b</sup> and Carmel Majidi\*<sup>a</sup>

<sup>a</sup> Department of Mechanical Engineering, Carnegie Mellon University, Pittsburgh, PA 15213, USA

<sup>b</sup> School of Chemical Engineering, Sungkyunkwan University (SKKU), Suwon 16419, Republic of Korea

<sup>c</sup> Human-Computer Interaction Institute, Carnegie Mellon University, Pittsburgh, PA 15213, USA

<sup>d</sup> Department of Semiconductor and Display Engineering, Sungkyunkwan University (SKKU), Suwon, 16419, Republic of Korea

<sup>e</sup> Mechanical Engineering, University of California, Berkeley, CA 94720, USA

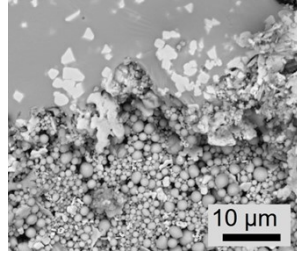


**Figure S1.** The SEM image of the boundary between sintered and non-sintered LM.

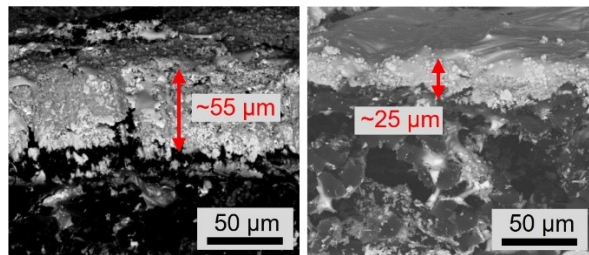


**Figure S2.** The cross-sectional SEM images of the LM-coated textile before (left) and after (right) applying pressure and undergoing sintering.

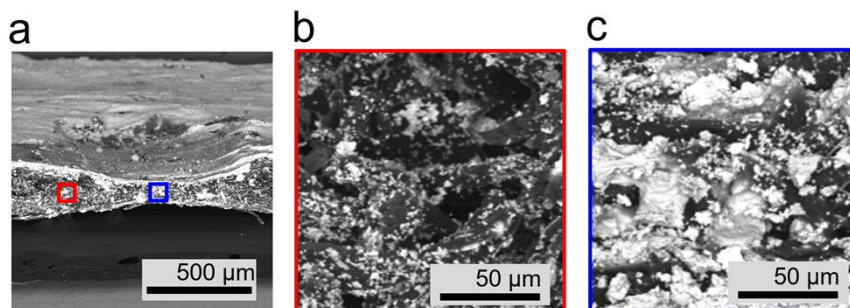


**Figure S3.** The cross-sectional sintered LM distribution SEM images. (a) The textile where high pressure is applied collapses and becomes thinner. (b) LM at the center of the textile, where no pressure is applied, exhibits sparse LM particle distribution. (c) LM is sintered and connected to each other, becoming conductive.

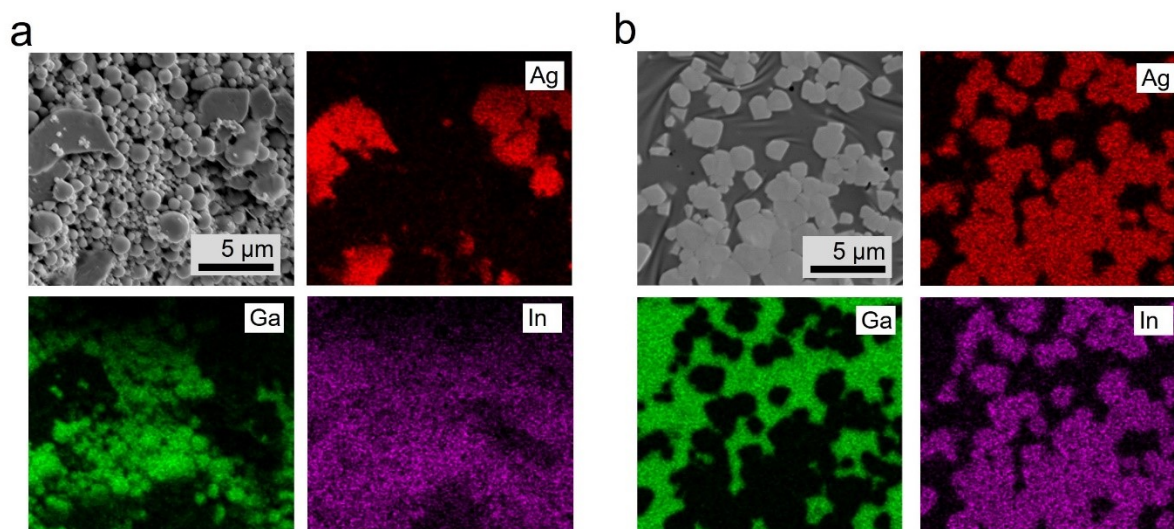


**Figure S4.** The SEM and EDS data of the LM and SF coated textile. (a) Images before the LM sintering and (b) after sintering. Red, blue, and green indicate Ag, Ga, and In, respectively.

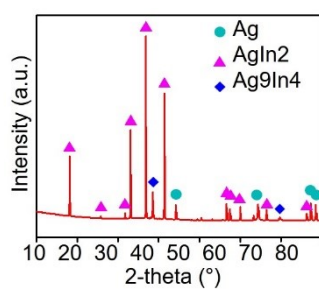


**Figure S5.** X-ray diffraction (XRD) pattern of LM/SF-coated textile, demonstrating the formation of Ag-In intermetallic compounds.

**Table S1** Comparison of liquid metal-based circuit designs from previous studies, highlighting the challenges of implementing double-sided circuits.

Layer Configuration	Composition	Fabrication Method	Notes	Ref.
Single layer	Ga + Fe	Magnetic Sintering	-	[49]
Single layer	Galinstan + Cu	Reactive Wetting	-	[50]
Single layer	eGaln + AgNP	Rubbing Deposition	-	[51]
Single layer	Galn + Ag + PVA	Nozzle Printing	-	[52]
Single layer	eGaln+TPU	Pressed Sintering	-	[53]
Double-sided	eGaln+PU	Acoustic Field	Vial hole	[54]
Double-sided	eGaln+Ag flake+SIS	Nozzle Printing	Deposit insulation layer	[55]
Double-sided	eGaln+Ag flake	Pressed Sintering	Controlled pressure	Our work

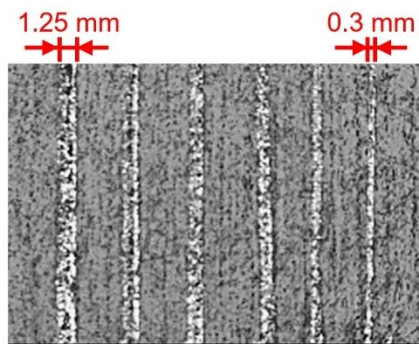


**Figure S6.** An optical image of the diverse circuit widths. The controllable smallest width is 0.3 mm.

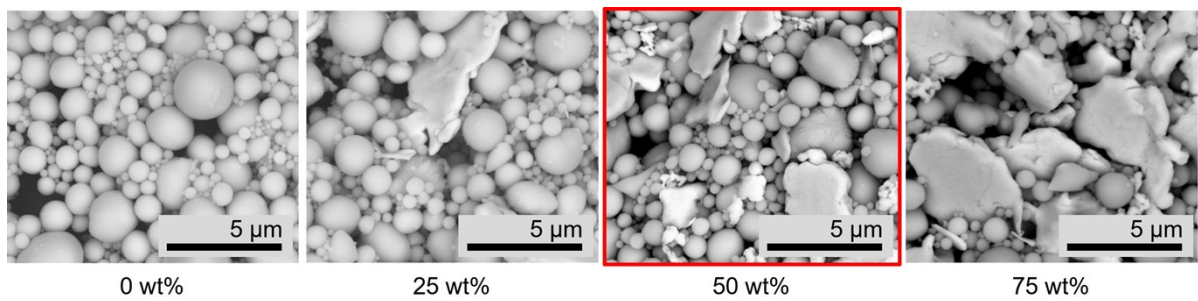


**Figure S7.** The 10k $\times$  magnified SEM images of LM particles with different ratios of SF. The experiment utilized the 50 wt% ratio, highlighted in the red box.

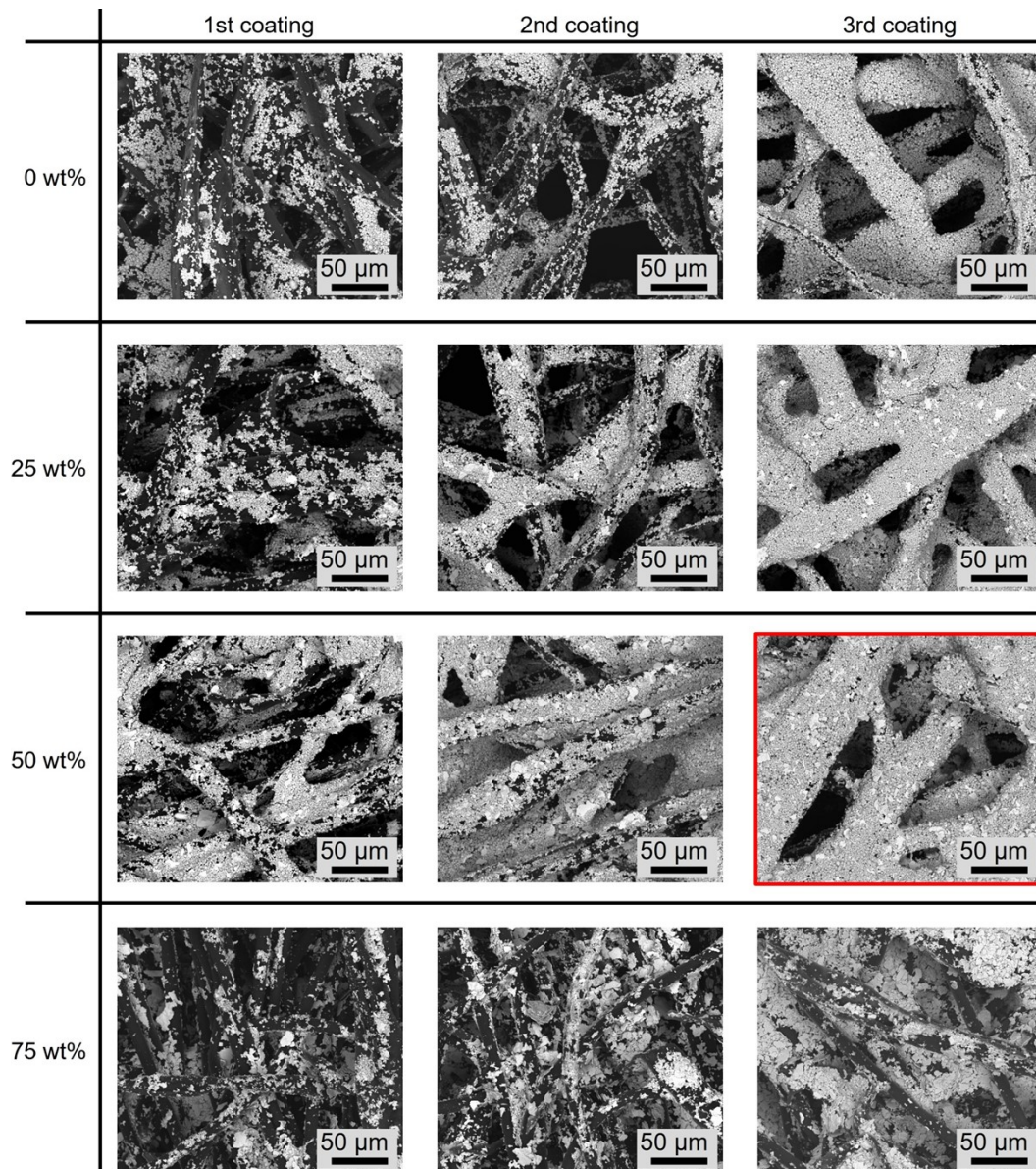


**Figure S8.** The 500× magnified SEM images of LM particles and SF-coated textile. The coated conditions vary depending on the number of coatings and the SF contents. The red box highlights the three times coating with 50 wt% SF, exhibiting the best performance.

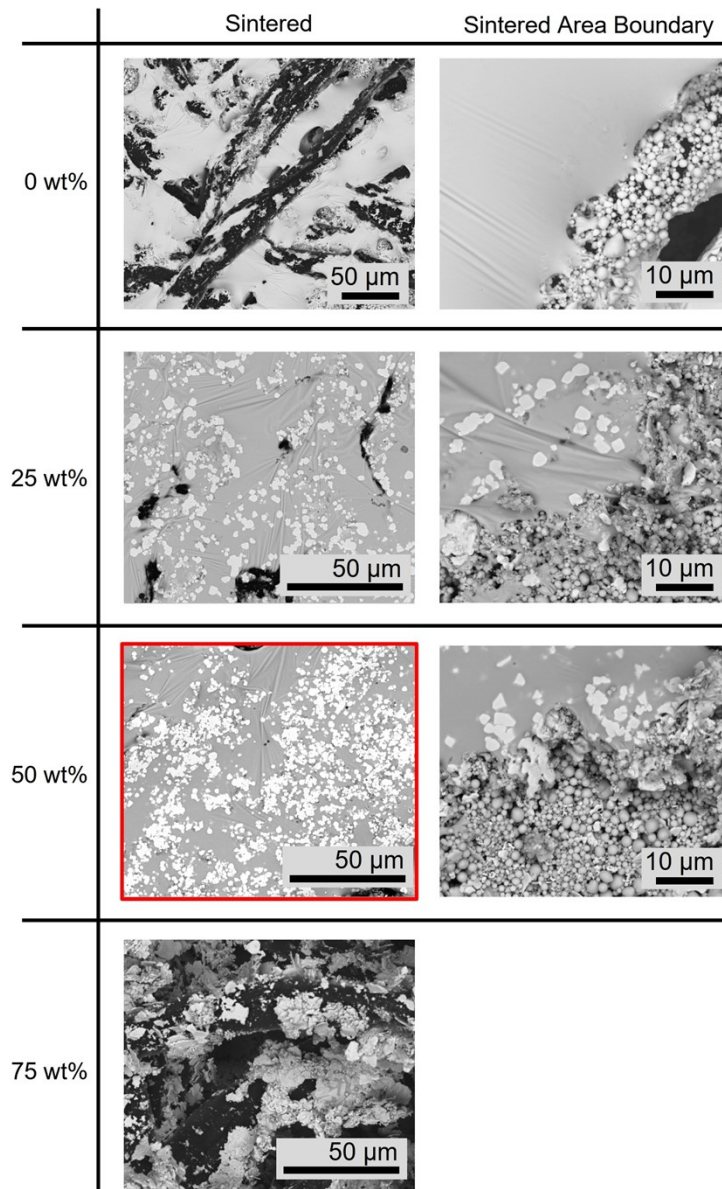


**Figure S9.** The SEM images when three times coated textile with different SF contents were sintered and their boundary. The LM and SF at 50 wt% textile, red box, were densely sintered with the best quality. The 75 wt% textile showed no adhesivity between fibers and metals.

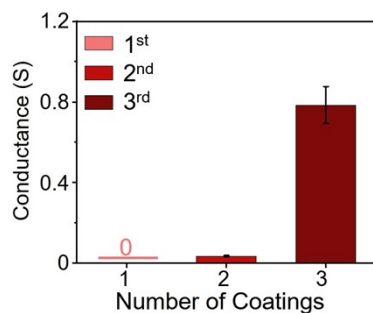


**Figure S10.** The conductance of textiles coated with 50 wt% SF depending on the number of coatings.

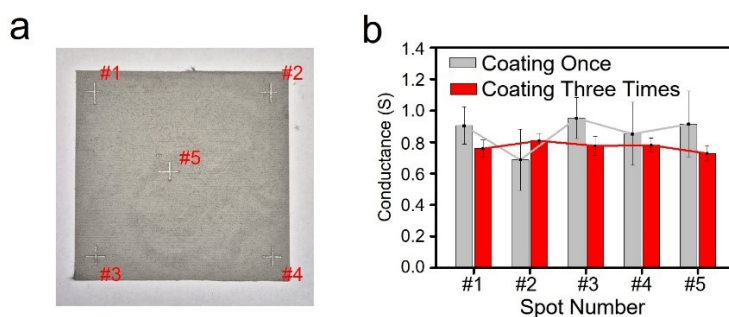


**Figure S11.** Coating uniformity test based on the position on the smart textile. (a) An image indicating measurement points on an 11 cm  $\times$  11 cm smart textile. (b) A graph showing conductance uniformity by position comparing single-coating and three-step coating methods.

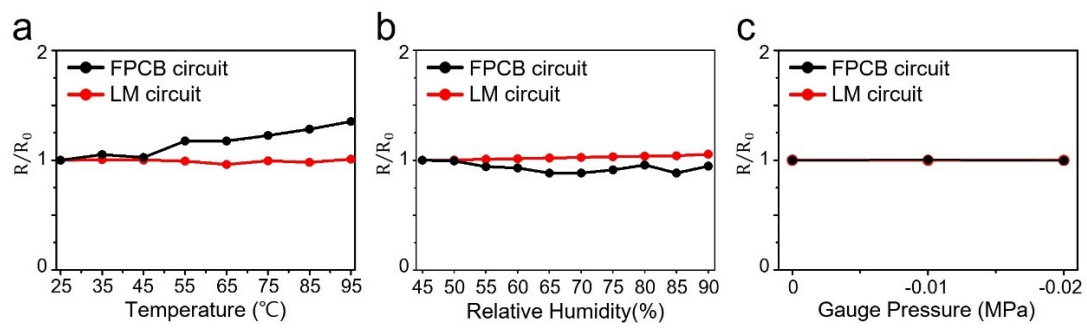


**Figure S12.** Stability under external environmental factors: (a) temperature, (b) humidity, and (c) pressure.

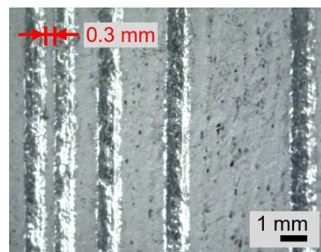


**Figure S13.** An optical image of the parallel circuits at various intervals. The closest gap is 0.3 mm.

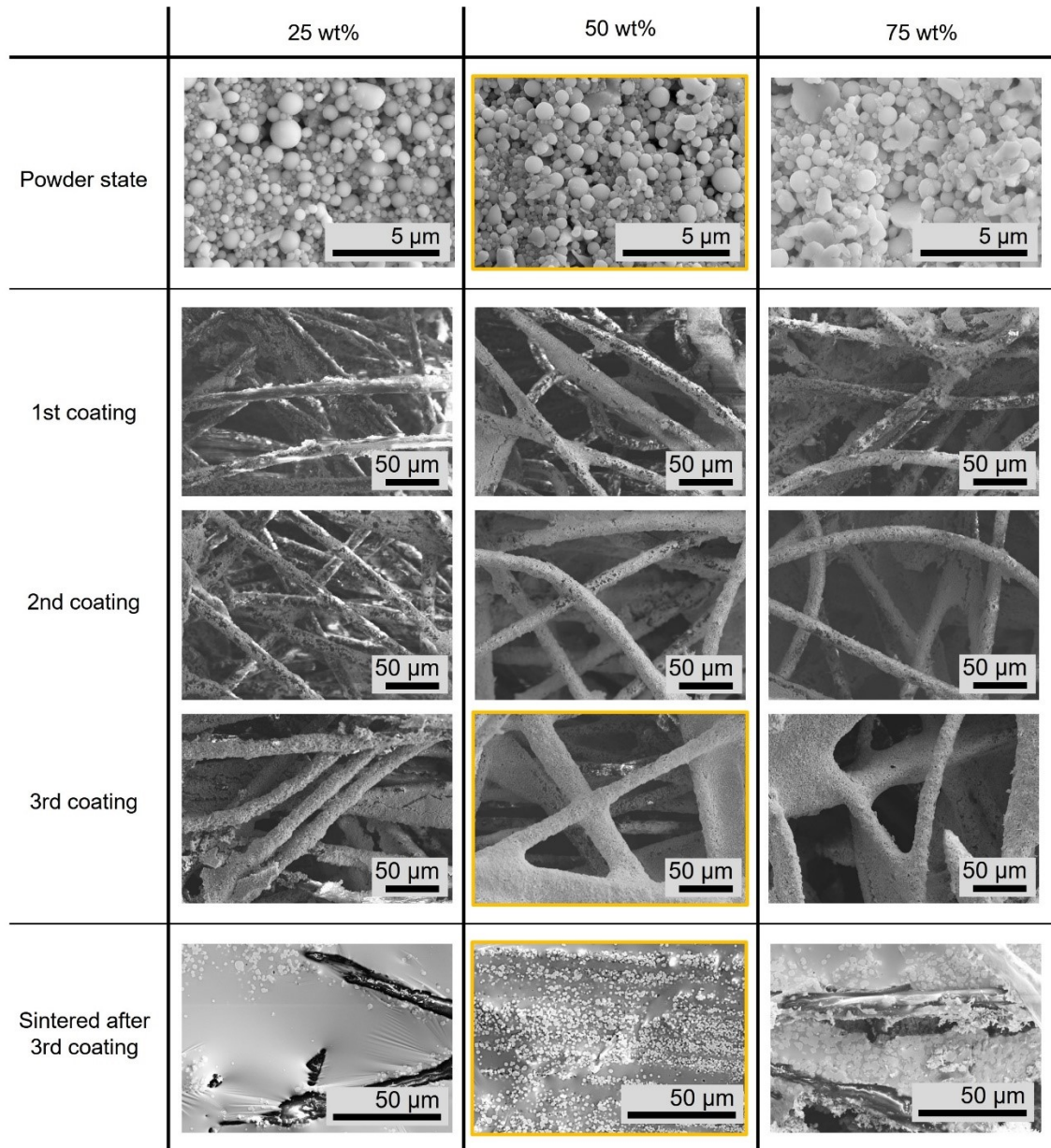


**Figure S14.** SEM images showing the powder state, coating condition, and post-sintering state based on the ratio of LM to SF91 (average size = 3.22  $\mu\text{m}$ ). In terms of coating condition, both the 50 wt% and 75 wt% ratios after three coatings appear satisfactory. However, based on the post-sintering state, only the 50 wt% ratio (yellow box) seems effective.

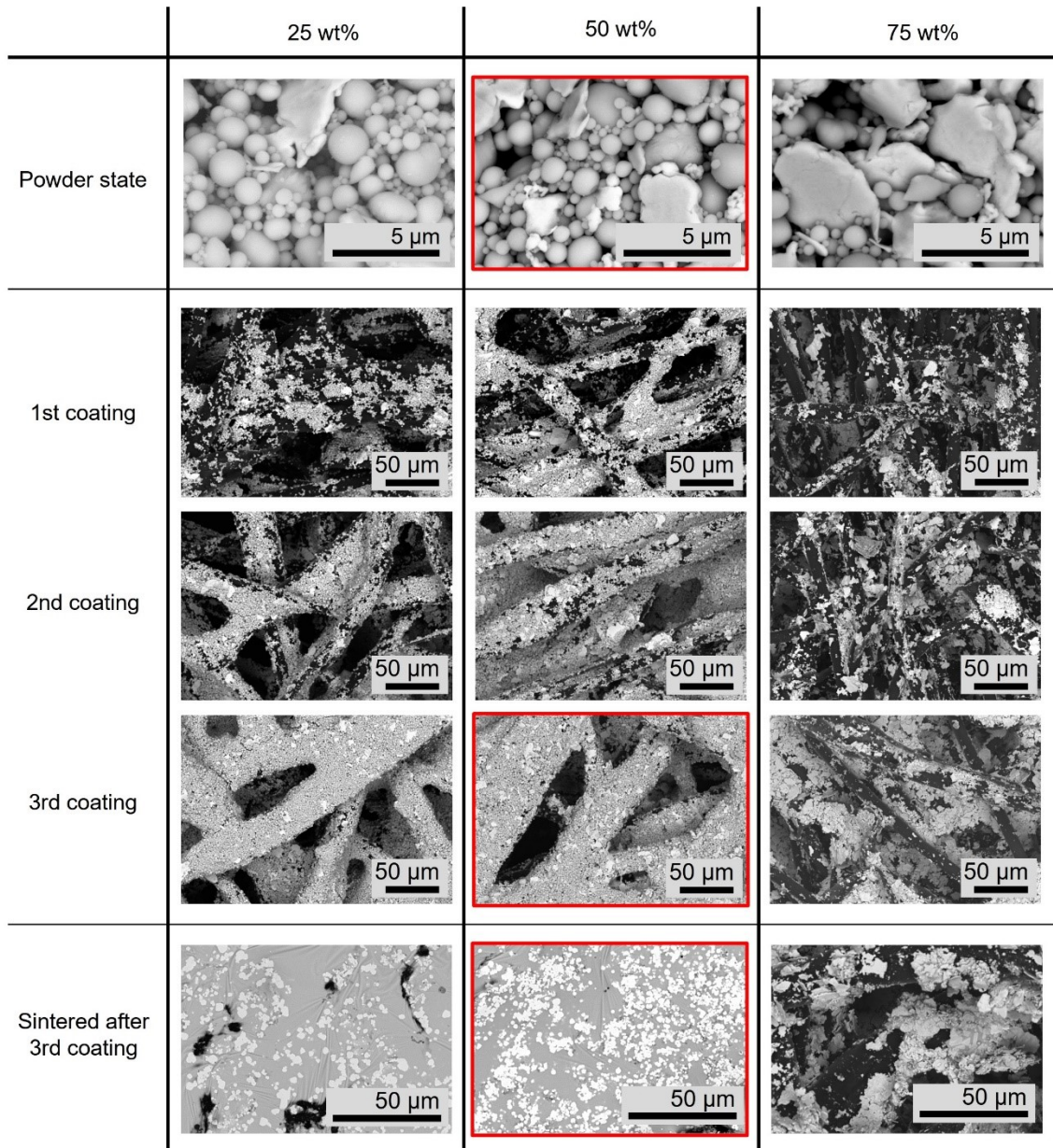


**Figure S15.** SEM images showing the powder state, coating condition, and post-sintering state based on the ratio of LM to SF94 (average size = 5.86  $\mu\text{m}$ ). In terms of coating condition, both the 25 wt% and 50 wt% ratios after three coatings appear satisfactory. However, after sintering, the 50 wt% ratio (red box) maintains a cleaner and more consistent structure.

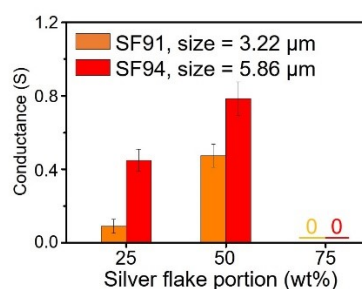


**Figure S16.** Comparison of conductance for SF91 and SF94 at 25 wt%, 50 wt%, and 75 wt% LM-to-SF ratios. All data were obtained after three coating cycles.

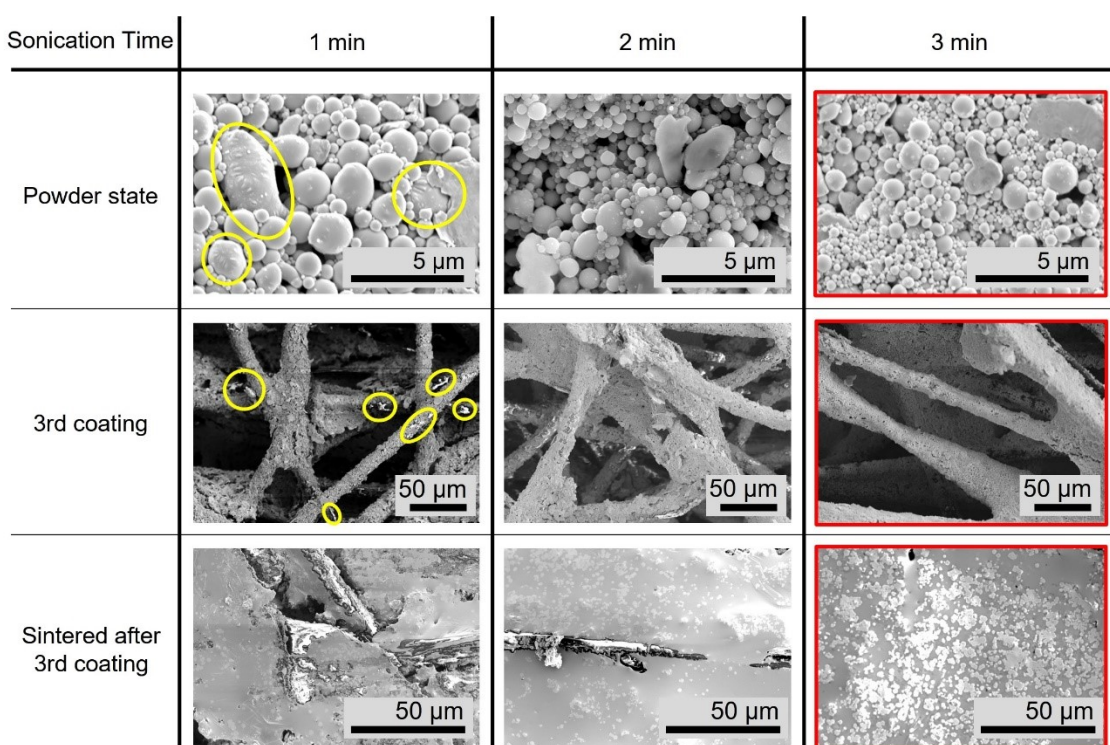


**Figure S17.** Differences in the fabricated smart textile based on sonication time. At 1 minute, particles are not fully formed, leaving liquid-state clusters (highlighted with yellow circles). At 2 minutes, relatively larger particles are present, resulting in a less smooth surface after coating. The larger particle size also reduces the interaction between LM particles and SF, leading to lower adhesion. Consequently, the smart textile fabricated at 3 minutes demonstrates optimal conditions with uniform coating and high adhesion.

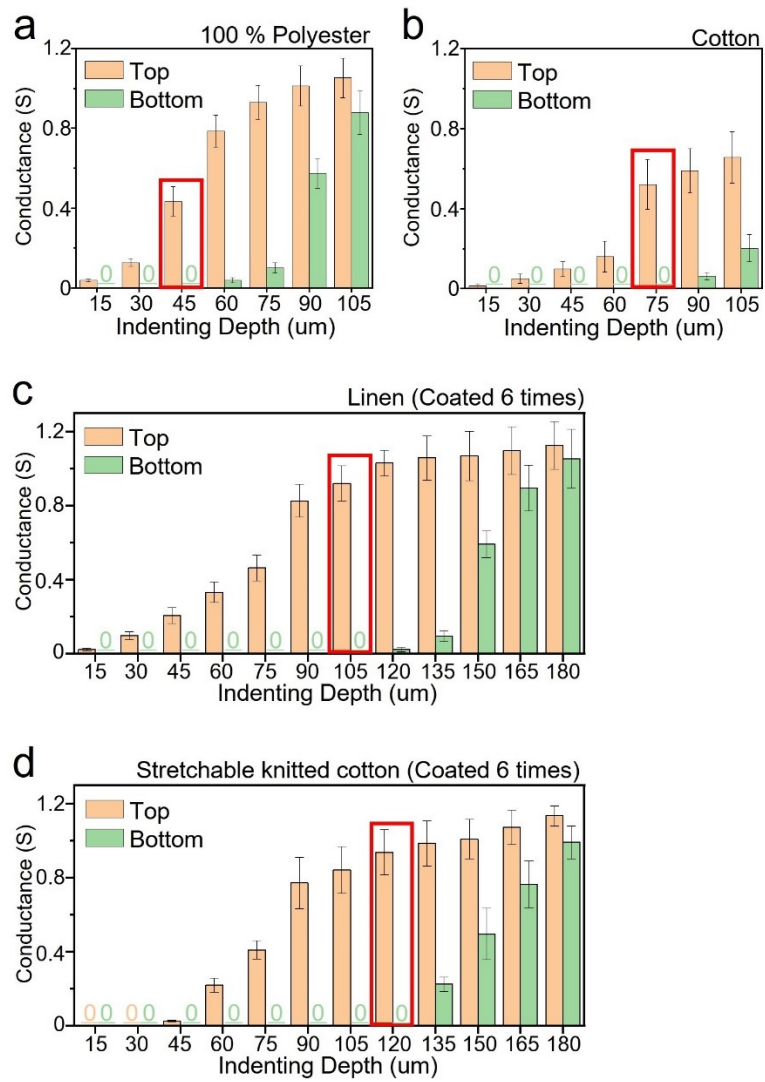


**Figure S18.** The electrical conductance of the different types of circuit-designed textiles. (a) 100 % polyester, (b) cotton, (c) linen, and (d) stretchable knitted cotton. For linen and knitted cotton, the coating process was performed 6 times.

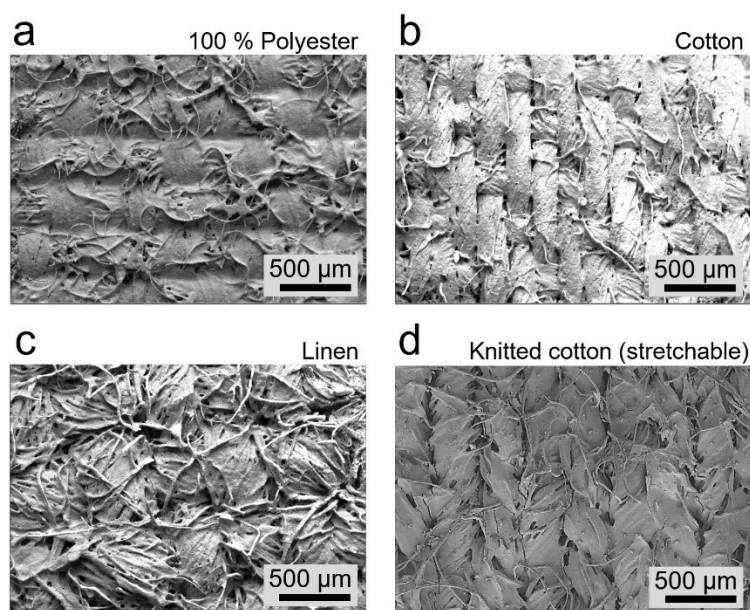


**Figure S19.** 50× magnified SEM images of the metal coated (a) 100 % polyester, (b) cotton, and (c) linen, and (d) stretchable knitted cotton. Linen and knitted cotton were coated 6 times, while polyester and cotton were coated 3 times each.

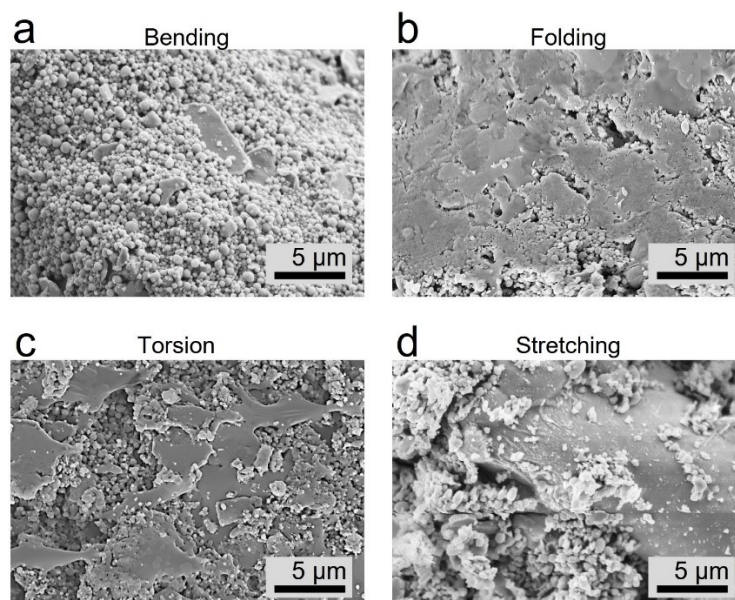


**Figure S20.** 5.0k × magnified SEM images of the LM particles after external deformations. (a) bending at a radius of 2.5 mm, (b) folding with a radius below 500 μm, (c) 360° torsion, and (d) 20 % stretching. Stretching was performed with the stretchable knitted cotton.

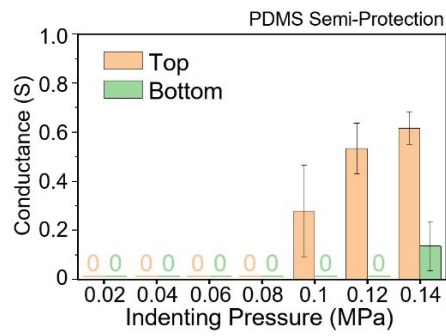


**Figure S21.** Conductance based on indenting pressure on PDMS semi-protection.

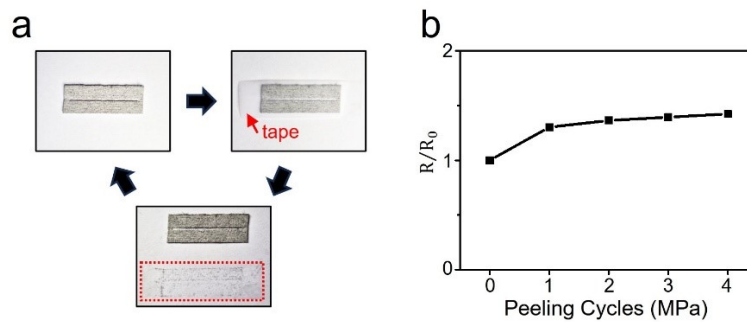


**Figure S22.** Particle detachment test using tape. (a) Testing method. Attaching and removing fresh tape to the smart textile a total of four times. (b) A graph showing relative resistance changes over cycles.

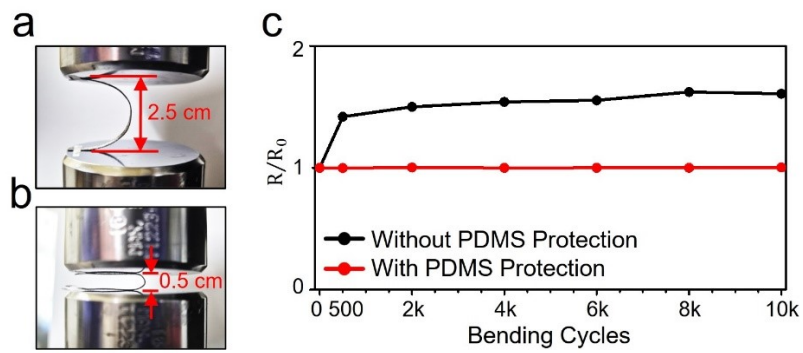


**Figure S23.** Durability test based on the presence of protection. (a) Initial state before bending, diameter = 2.5 cm. (b) Post-bending state, diameter = 0.5 cm. (c) A graph showing relative resistance changes over 10k bending cycles.

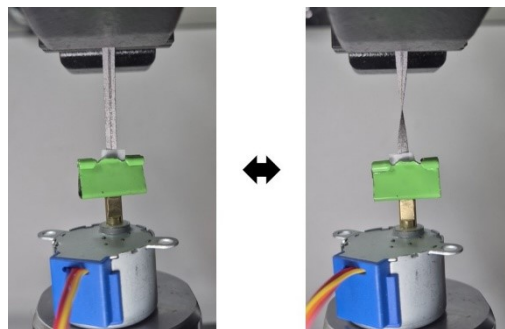


**Figure S24.** Experimental setup for the torsion test. One end of the smart textile is fixed, while the other end is attached to a stepper motor that rotates from  $-180^\circ$  to  $180^\circ$ .

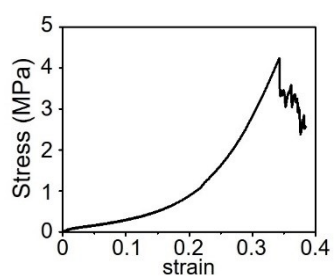


**Figure S25.** Stress-strain curve of the LM-coated smart textile under tensile loading, demonstrating nonlinear elastic behavior followed by peak stress and subsequent failure.

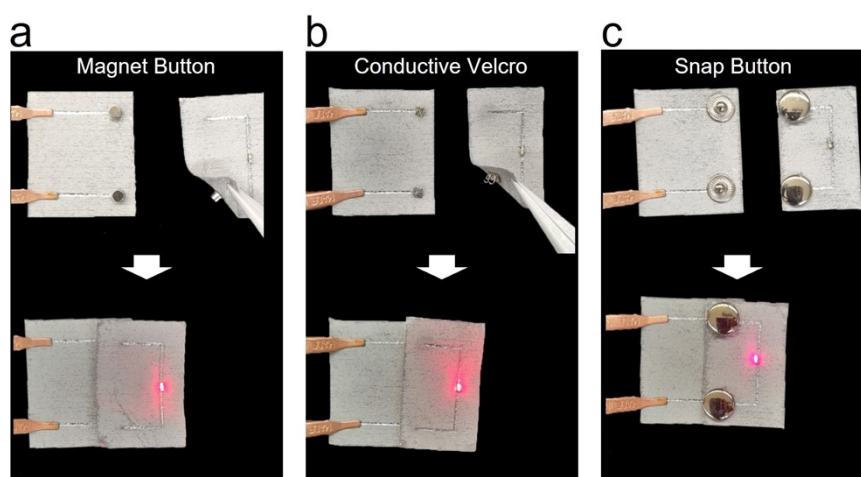


**Figure S26.** Various types of conductive buttons. (a) Magnet button, (b) conductive Velcro, and (c) conductive snap button.

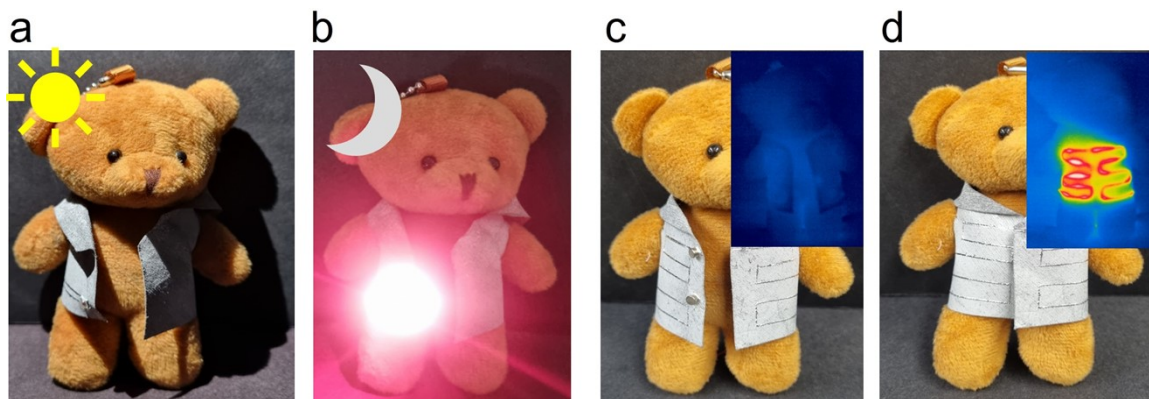


**Figure S27.** Teddy bear's reversible cloth before color painting. (a-b) Activation of LED depending on the brightness. (c-d) Joule heating operation when buttoned up.